



ELSEVIER

Computer Physics Communications 147 (2002) 684–689

Computer Physics
Communications

www.elsevier.com/locate/cpc

Numerical simulations of random spin (and fermionic) models with a wide distribution of energy scales [☆]

R.N. Bhatt ^{a,*}, Xin Wan ^b, Malcolm P. Kennett ^c, Mona Berciu ^a

^a Princeton University, Department of Electrical Engineering, Princeton, NJ 08544-5263, USA

^b Florida State University, Department of Physics, Tallahassee, FL 32306, USA

^c Princeton University, Department of Physics, Princeton, NJ 08544-0708, USA

Abstract

The magnetic behavior of semiconductors doped with randomly distributed magnetic elements (such as iron or manganese) and/or bound carriers (such as phosphorus or boron in silicon) are described by many-body Hamiltonians with a broad distribution of coupling constants and energy scales. These wide distributions (covering several orders of magnitude in some cases) lead to unusual properties, such as strong suppression of magnetic phase transitions due to quantum fluctuations, unusual thermodynamic behavior in the magnetically ordered phase, etc. The wide distributions also pose several challenges to both analytical and computational approaches used to calculate the physical properties of such systems. We describe some of the techniques that have been applied successfully to such systems, including numerical renormalization group as well as Monte Carlo methods. Examples are drawn from lightly doped conventional semiconductors [Si, Ge] as well as diluted magnetic semiconductors [such as (Cd,Mn)Te and (Ga,Mn)As]. Extension of these methods to diluted magnetic semiconductors in the metallic regime with itinerant carriers (fermionic degrees of freedom) is also discussed. © 2002 Elsevier Science B.V. All rights reserved.

Keywords: Doped semiconductors; Diluted magnetic semiconductors; Magnetic properties; Monte Carlo simulations

1. Introduction

Semiconductors containing a small amount of impurities offer a unique system in which several phenomena of interest to many-body physics can be observed in a rather clean way. Because the Bohr radius describing the (hydrogenic) wavefunction of the carrier provided by the dopant can vary from atomic scale to several hundred Å, a wide range of behavior, not possible in other materials, is actually observed

in such systems. (The extra length scale, distinct from the lattice scale, allows the greater degree of flexibility.) Thus, doped semiconductors form ideal materials to study the phase transition [1] from an insulator (at low doping densities) to a metal (at high doping densities). Concomitantly, there are large changes in transport, optical as well as magnetic behavior. We concentrate on this last aspect in this paper. It is extremely important to recognize that the system of impurities is randomly (Poisson) distributed; consequently, many of the ideas coming out of periodic lattice systems do not apply here.

In Section 2, we discuss doped nonmagnetic semiconductors, and show how the magnetic properties at

[☆] This research was supported by NSF DMR-9809483.

* Corresponding author.

E-mail address: ravin@ee.princeton.edu (R.N. Bhatt).

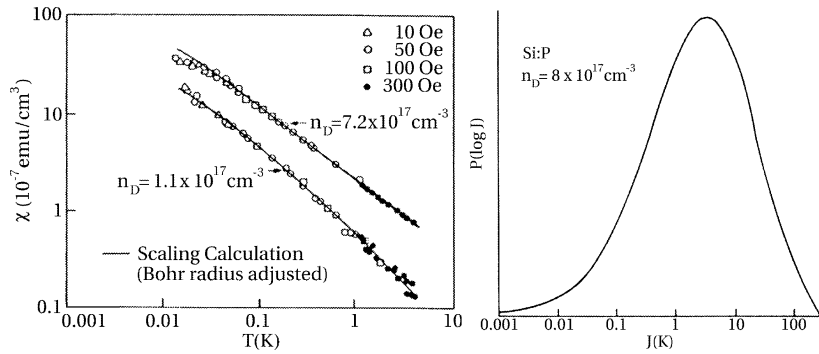


Fig. 1. Left: Low-temperature magnetic susceptibility of Si:P in the insulating phase. Points correspond to data [3] and solid lines are calculations from Ref. [2]; Right: Probability distribution of the initial (bare) nearest-neighbor exchange coupling at the density indicated.

low doping densities, in particular, led to an understanding of the significant effect of large-scale disorder (broad distribution of coupling constants) in quantum mechanical systems. The next two sections pertain to diluted magnetic semiconductors (DMS), where the host semiconductor is an alloy with a small percentage of the sites replaced by a magnetic ion (e.g., Mn) with a magnetic moment in the ground state arising from an unfilled *d*-shell. The presence of the magnetic ion leads to a reversal of the magnetic nature of the doped semiconductor from antiferromagnetic (AFM) to ferromagnetic (FM); however, the two families share the aspect of a broad spectrum of energy scales over which magnetic and thermodynamic degrees of freedom remain active. We discuss the consequences of the broad distributions in each of these systems (compared to typical condensed matter systems with zero or weak disorder), as well as the challenges faced by different computational methods to address the problem.

2. Antiferromagnetic systems

For nonmagnetic semiconductors (e.g., Si, Ge) containing either n-type (P or As) or p-type (B or Ga) impurities, the magnetic properties at low temperatures (*T*) are determined mostly by the carriers bound to the impurities. At very low concentrations (*n*) these bound carriers act as free spins, giving rise to a Curie ($\chi_c = C/T$) susceptibility. However, as *n* is raised or *T* lowered sufficiently, interactions between the bound carriers come into play. Interactions between electrons

bound in hydrogenic states are described by a Heisenberg exchange Hamiltonian [2]:

$$H = \sum_{i,j} J(\mathbf{R}_{ij}) \mathbf{s}_i \cdot \mathbf{s}_j, \tag{1}$$

where *i* and *j* are the random dopant positions and $J(R) \sim \exp(-2R/a_B)$ is the AFM exchange interaction. The resultant χ is lower [3] than the Curie value (see Fig. 1, left panel). However, one major surprise is that unlike other known materials with (random) magnetic interactions, this system shows no sign of a phase transition to a globally ordered state where the spins are aligned in even a random configuration that is fixed in time, down to *T* well below typical *J*.

The understanding of why that happens was provided by Bhatt and Lee [2], who showed, using a numerical position space perturbative renormalization group (RG) scheme, that for a system where the interactions are distributed very broadly (over several orders of magnitude, see Fig. 1, right panel), quantum fluctuations prevent ordering down to *T* several orders of magnitude below that of a classical Ising system with the same distribution of coupling constants [4]. The broad distribution turns out to be crucial for the scheme to work—the perturbative parameter is the ratio between the typical and maximum interactions at every stage of the RG procedure. As long as the distribution remains broad, the perturbative approach is extremely good quantitatively [2]. The dominance of antiferromagnetic interactions, which lead to magnetically inert singlet (non-degenerate) ground states for strongly coupled spins, is also a prerequisite for this

approach to work. Monte Carlo methods have been applied to similar problems in one-dimension [5], but do not appear to be competitive with the numerical RG approach. The main unexpected result is that the magnetic response at low temperature is dominated not by long wavelength spin excitations, as in a homogeneous system, but instead by dopant spins in unlikely spatial configurations, such that their effective interactions with the surroundings are strongly weakened as a result of the renormalization scheme. Interestingly, these effects persist into the metallic phase at higher doping densities, where instead of a T -independent Pauli susceptibility, a strongly T -dependent $\chi(T)$, potentially diverging as $T \rightarrow 0$ is seen [6,7], apparently due to similar phenomena.

3. Ferromagnetic systems: II–VI DMS

In diluted magnetic semiconductors, the interactions between the carrier spins and the magnetic ions overwhelm the antiferromagnetic interactions among the carriers in the regime of interest, leading to an (essentially) ferromagnetic phase at low T . Conventional ferromagnets are qualitatively well described by a Weiss (mean-field) treatment of the Heisenberg Hamiltonian $H = \sum_{i \neq j} J_{ij} \mathbf{S}_i \cdot \mathbf{S}_j$. For spins \mathbf{S}_i arranged on a lattice, the mean-field critical temperature is $T_C = |J|S(S+1)/3k_B$, where $J = \sum_{j \neq i} J_{ij}$ and S is the magnitude of the spin. Below T_C , the spontaneous magnetization $\langle M \rangle = g\mu_B \langle S_i^z \rangle$ increases rapidly (Fig. 2), and it is close to the saturation value $M_0 = g\mu_B S$ below $T < 0.5T_C$. While fluctuation effects make quantitative changes, $M(T)$ retains most of its variation near T_C , and the qualitative shape of the curve remains as in the Weiss treatment. Concurrently, the specific heat has a peaked structure around T_C , and drops rapidly to zero for $T < 0.5T_C$ reflecting the fact that the only accessible degrees of freedom for low T are the long-wavelength (collective) spin-wave excitations with low phase space.

A typical II–VI DMS system is a semiconductor such as CdTe or ZnSe, with some of the divalent sites (Cd/Zn) substituted by the magnetic ion Mn, which is isovalent with Cd/Zn, but also has a half-filled 3d shell, with an $S = 5/2$ spin (Hund's rule). For small concentrations x of Mn, direct interactions between the Mn spins can be neglected. When shallow (charged)

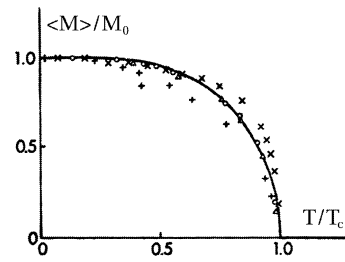


Fig. 2. Magnetization of a Weiss ferromagnet as a function of temperature (solid line). The experimental points are for iron (x), nickel (o), cobalt (Δ) and magnetite (+) [8].

dopants are introduced in the system, the bound electron (or hole) in a hydrogenic 1s state interacts with the $S = 5/2$ Mn spins via an exchange interaction of the Heisenberg type, leading to a Hamiltonian [9]:

$$H = \sum_{i,j} J(\mathbf{r}_i, \mathbf{R}_j) \mathbf{s}_i \cdot \mathbf{S}_j. \quad (2)$$

The exchange interaction $J(\mathbf{r}_i, \mathbf{R}_j)$ between the electron/hole centered at \mathbf{r}_i and the Mn spin at \mathbf{R}_j is proportional to the electronic charge density at the Mn site, which, for hydrogenic 1s wavefunctions leads to

$$J(\mathbf{r}_i, \mathbf{R}_j) = J_0 e^{-2|\mathbf{r}_i - \mathbf{R}_j|/a_B}, \quad (3)$$

where J_0 is the exchange constant and a_B is the Bohr radius (~ 10 – 20 \AA). Typically, for electrons $J_0 < 0$, while for holes $J_0 > 0$. However, since in the following we treat the spins as classical variables, the sign is irrelevant. For specificity, in the rest of the paper we assume $J_0 > 0$.

Qualitatively, at a temperature $k_B T < J(r)$ [see Eq. (3)], all Mn spins within distance r of a dopant will order their spins antiferromagnetically with respect to the dopant hole spin, creating a region with a large moment (from all the parallel polarized Mn spins) near the dopant, known as a bound magnetic polaron (BMP). The radius of the BMP increases with decreasing T , leading to true long-range FM order when T is low enough that a continuous percolating network of BMPs is formed. However, since the corresponding percolation fraction is $\sim 20\%$, even below the transition many Mn spins remain unattached to the percolated cluster till much lower T . This results in a very unusual FM phase, in which a substantial part of the spin entropy survives down to very low T .

We performed Monte Carlo simulations on the Hamiltonian (2) to study this unusual FM phase, treat-

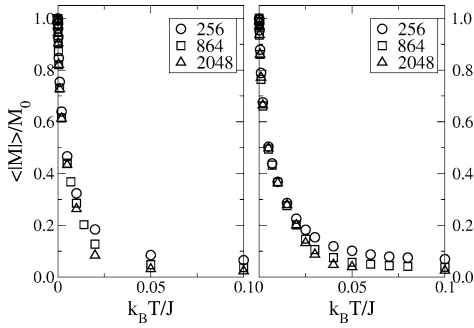


Fig. 3. Magnetization per Mn spin as a function of temperature, in a II–VI DMS, for classical/discrete spin models (left/right panel). The magnetization curves are very unlike the typical magnetization curve shown in Fig. 2.

ing both Mn and carrier spins as classical variables. This appears to be a reasonable approximation since $S = 5/2$ is a large spin and the Mn spins dominate the magnetic response. We used the standard single-spin-flip Metropolis algorithm satisfying detailed balance at each step. Equilibration was achieved [10] by running two copies with identical locations for dopants and Mn spins. One copy was initialized with a totally random configuration of spins, and the other one with the expected $T = 0$ FM ground state configuration. Measurements were made after the magnetization $\langle |M| \rangle$ of the two replicas agreed within error bars.

Simulations were carried out for zinc-blende lattices with lattice constant $a = 5 \text{ \AA}$, for Mn concentration $x = 0.001$, dopant density $n_d = 10^{18} \text{ cm}^{-3}$ and $a_B = 20 \text{ \AA}$. The exchange J_0 defines the unit of energy. Lattices with linear sizes 20–40 were considered, with 256–2048 Mn spins and 8–64 carrier spins, respectively, averaging up to 3000 samples [11]. The magnetization curves obtained have unusual, concave shapes (see Fig. 3, left panel), very unlike the typical magnetization curve of Fig. 2. For these parameters, the critical temperature $T_C = 0.014J_0$ is found using finite size scaling [11]. We find that the magnetization reaches its saturation value only at exponentially small temperatures, reflecting the existence of the quasi-free Mn spins outside the percolated (magnetically ordered) region.

Specific heat of the classical Heisenberg model has the unphysical limit $C_V \rightarrow Nk_B$ as $T \rightarrow 0$ (see Fig. 4). While this agrees with the equipartition theorem, it implies that quantum mechanics (discrete energy levels) is needed to capture the correct limit $C_V \rightarrow 0$

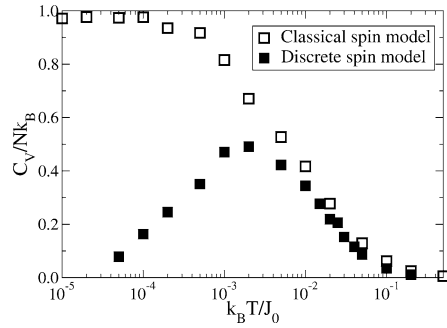


Fig. 4. Specific heat per Mn spin as a function of temperature, for continuous (empty squares) and discrete (full squares) spin models. $N = 2048$ Mn spins in both cases.

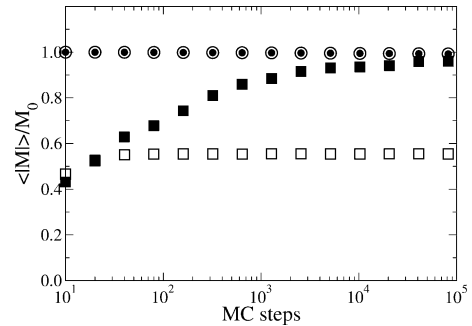


Fig. 5. Equilibration times for two replicas with 256 spins, starting with random spin configuration (squares), and with FM spin configuration (circles), for $k_B T / J_0 = 10^{-5}$. Empty (full) symbols correspond to the single-spin-flip (cluster) algorithm.

as $T \rightarrow 0$. One way to mimic the discretization, but avoid the complexities of the quantum Monte Carlo treatment, is to use a discrete (classical) vector model, in which each Mn spin can only be oriented along one of the six [100] directions. In this case the single-spin-flip approach cannot be used, especially at T small compared to the (finite) energy needed for a spin-update. At such T , samples freeze in metastable states, with BMPs polarized in different directions, and equilibration times become extremely long. An efficient cluster algorithm allowing the flipping of entire domains of polarized spins at once has been implemented in this case (for details, see Ref. [11]), leading to much faster equilibration times (see Fig. 5).

While the magnetization curves are very similar to the ones obtained in the continuous spin Heisenberg model (see Fig. 3), the specific heat results are very different (see Fig. 4). As expected, for the discrete

model $C_V \rightarrow 0$ as $T \rightarrow 0$. However, unlike for a typical FM, the peak in C_V is not near T_C , but at temperatures well below T_C . This is a reflection of the residual entropy of the free Mn spins outside the percolated region.

4. Ferromagnetic systems coupled to fermions: III–V DMS

When Mn is doped in a III–V semiconductor, such as GaAs, the major difference with respect to the II–VI DMS is that the Mn atom provides both the $S = 5/2$ spin and the dopant charge carrier (a hole, since Mn, of valence II, substitutes for Ga, of valence III). While this implies equal numbers of holes and Mn spins, it is experimentally found that the holes to Mn spins ratio is $p = 10\text{--}30\%$.

For low Mn concentrations x , it is again useful to start from the single-dopant limit, and assume that holes are trapped in hydrogen-like impurity states about Mn atoms. However, since the number of holes is smaller than the number of Mn, there must be a mechanism to allow the holes to “choose” the Mn dopants near which to stay. Such a mechanism is naturally provided by hopping processes facilitated by the overlap between impurity wave functions centered at different Mn sites. Thus, the simplest Hamiltonian describing this system is

$$H = \sum_{i \neq j} t_{ij} c_{i\sigma}^\dagger c_{j\sigma} + \sum_{i,j} J_{ij} \mathbf{s}_i \cdot \mathbf{S}_j. \quad (4)$$

Here, i indexes different Mn positions \mathbf{R}_i , and $c_{i\sigma}^\dagger$ is the creation operator for a hole of spin σ in the impurity level centered at \mathbf{R}_i . The first term describes hopping of holes between impurity levels. If (for simplicity) we again assume 1s impurity states, $t_{ij} = 2(1 + r/a_B) \exp(-r/a_B) \text{ Ry}$, where $r = |\mathbf{R}_i - \mathbf{R}_j|$ [12]. The Bohr radius $a_B = 7.8 \text{ \AA}$ and the binding energy $1\text{Ry} = 110 \text{ meV}$ for Mn in GaAs [13]. The second term describes the AFM coupling between the Mn spin \mathbf{S}_j and the hole spin $\mathbf{s}_i = \frac{1}{2} c_{i\alpha}^\dagger \sigma_{\alpha\beta} c_{i\beta}$ (σ are the Pauli spin matrices). As in II–VI DMS, the AFM exchange is proportional to the probability of finding the hole trapped at \mathbf{R}_i near the Mn spin at \mathbf{R}_j , $J_{ij} = J \exp(-2|\mathbf{R}_i - \mathbf{R}_j|/a_B)$ [see Eq. (3)]. For Mn in GaAs, $J = 15 \text{ meV}$ [13].

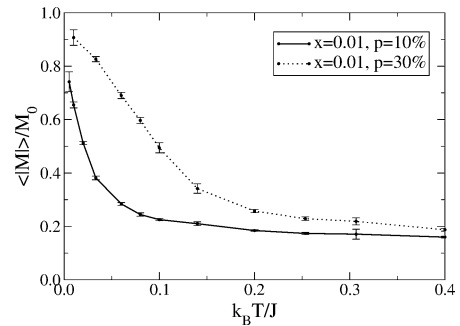


Fig. 6. Magnetization per Mn spin as a function of temperature, in a III–V DMS. Curves correspond to $x = 0.01$, and relative holes to Mn concentrations $p = 10$ and 30%.

We have investigated the Hamiltonian (4) using Monte Carlo methods. The Mn spins \mathbf{S}_j are again treated as classical variables. Since the Hamiltonian is quadratic in hole operators, it can be diagonalized for any configuration of Mn spins \mathbf{S}_j and the free energy of the holes can be computed. This allows us to decide whether individual Mn spin flips are accepted, using the Metropolis algorithm. In each Monte Carlo step we reupdate each Mn spin once, and we average the final results over many realizations of Mn disorder. Again, comparisons between initially fully polarized and initially completely random samples are used to determine the equilibration times. However, there are some complications due to the fact that the Mn spins do not interact directly (as in traditional spin Hamiltonians), but through the fermionic degrees of freedom. One complication is related to finding a proper value for the chemical potential μ for a desired hole density. A second complication is due to the fact that numerical diagonalization of the Hamiltonian after each individual spin flip is too time-consuming. We have implemented a perturbational scheme to compute the change in the hole-free energy due to a spin flip, and we use full diagonalization after each Monte Carlo step to re-update the hole eigenfunctions and eigenenergies. This algorithm is described in Ref. [14].

The magnetization curves (see Fig. 6) have unusual concave shapes, similar to the ones obtained for the II–VI DMS (see Fig. 3). However, the critical temperatures (found from finite size scaling [14]) are comparatively much larger than in II–VI DMS. The increased T_C is due to the fact that hole wavefunctions in the III–V DMS are peaked at the Mn sites, and

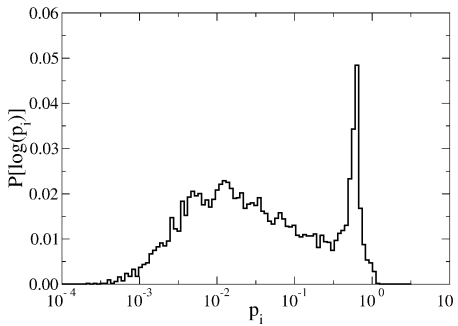


Fig. 7. Histogram of probability p_i to find a hole at Mn site \mathbf{R}_i , at $k_B T/J = 0.01$, for $x = 0.01$ and relative hole to Mn concentration $p = 10\%$.

furthermore, holes are free to move through the system from one Mn impurity to another. As a result, they tend towards regions with larger than average local Mn concentration, where they can lower both their kinetic and magnetic energy. Since the AFM coupling to Mn spins is proportional to the probability of finding the hole at the Mn site, the effective coupling for Mn spins in these regions is substantially increased, leading to higher polarization temperatures for the spins in these regions. (In contrast, in a II–VI DMS, the holes are localized near their dopants, and can only interact with the Mn spins that happen to be near their orbits). Holes traveling between various high-density polarized regions in a III–V DMS force the alignment of Mn spins in all regions to be the same, in order to minimize their kinetic energy. This mechanism for the alignment of high-density polarized regions is also more effective than the one in II–VI DMS, where correlations between different BMPs are established through the weakly interacting spins in between the BMPs. Taken together, these effects explain the higher T_C of III–V DMS, in qualitative agreement with experimental observations, which have found $T_C < 4$ K in II–VI DMS, while $T_C = 110$ K for $\text{Ga}_{0.95}\text{Mn}_{0.05}\text{As}$.

The highly inhomogeneous distribution of holes among the Mn spins can be seen from a histogram of probabilities to find holes at various Mn sites. If the holes were equally distributed among the Mn sites, the probability to find a hole at any Mn site would be the same, $p = 0.10$ (for 90% compensation). From Fig. 7 we see that there is a very wide distribution of probabilities, from $p \sim 0.8$ for Mn in high-density regions, to $p \sim 10^{-2}$ or less in low-density regions. This is

simply a reflection of this highly inhomogeneous system, in which long-range magnetic order coexists with a large fraction of almost free (non-interacting) spins, leading to very unusual magnetic properties.

5. Conclusions

We have briefly discussed three families of semiconductor-based magnetic Hamiltonians. Because of the existence of multiple length scales—an effective Bohr radius of a shallow impurity state, which can be very different from atomic scales and lattice constants, all these systems are described by a wide distribution of coupling constants, which poses special challenges for numerical methods. Depending on whether the system is AFM or FM at low temperatures, numerical renormalization group or Monte Carlo methods appear to be more appropriate, and with proper care, appear to yield reliable results for the rather unconventional magnetic (and ensuing thermodynamic) properties.

References

- [1] N.F. Mott, *Metal Insulator Transitions*, Taylor and Francis, London, 1990;
- R.F. Milligan et al., in: A.L. Efros, M. Pollak (Eds.), *Electron–Electron Interactions in Disordered Systems*, 1985, pp. 231–286.
- [2] R.N. Bhatt, P.A. Lee, *Phys. Rev. Lett.* 48 (1982) 344;
- R.N. Bhatt, *Phys. Scripta T* 14 (1986) 7.
- [3] K. Andres et al., *Phys. Rev. B* 24 (1981) 244.
- [4] R.N. Bhatt, *Physica* 109–110B (1982) 2145.
- [5] J.E. Hirsch, R. Kariotis, *Phys. Rev. B* 32 (1985) 7320;
- H.-B. Schuttler et al., *Phys. Rev. B* 35 (1987) 3461.
- [6] M.A. Paalanen, *Phys. Rev. Lett.* 57 (1986) 2061;
- M.J. Hirsch et al., *Phys. Rev. Lett.* 68 (1992) 1418.
- [7] R.N. Bhatt et al., *J. Phys. C* 8 (1988) 1179;
- R.N. Bhatt, D.S. Fisher, *Phys. Rev. Lett.* 68 (1992) 3072.
- [8] R.K. Pathria, *Statistical Mechanics*, Pergamon Press, Oxford, 1972.
- [9] P.A. Wolff, R.N. Bhatt, A.C. Durst, *J. Appl. Phys.* 79 (1996) 5196.
- [10] R.N. Bhatt, A.P. Young, *Phys. Rev. B* 37 (1988) 5606.
- [11] R.N. Bhatt, X. Wan, *Int. J. Mod. Phys. C* 10 (1999) 1459;
- X. Wan, R.N. Bhatt, *cond-mat/0009161*.
- [12] R.N. Bhatt, *Phys. Rev. B* 24 (1981) 3630.
- [13] M. Berciu, R.N. Bhatt, *Phys. Rev. Lett.* 87 (2001) 107 203.
- [14] M.P. Kennett, M. Berciu, R.N. Bhatt, *cond-mat/0203173* (unpublished).